

Direct To Digital Holography For High Aspect Ratio Inspection of Semiconductor Wafers

C. E. (Tommy) Thomas Jr.^a, Martin A. Hunt^a, Tracy M. Bahm^a, Larry R. Baylor^b, Philip R. Bingham^b, Matthew D. Chidley^b, Xiaolong Dai^a, Robert J. Delahanty^a, Ayman El-Khashab^a, Judd M. Gilbert^a, James S. Goddard^b, Gregory R. Hanson^b, Joel D. Hickson^a, Kathy W. Hylton^b, George C. John^a, Michael L. Jones^a, Michael W. Mayo^a, Christopher Marek^a, John H. Price^a, David A. Rasmussen^b, Louis J. Schaefer^a, Mark A. Schulze^a, Bichuan Shen^a, Randall G. Smith^a, Allen N. Su^a, Kenneth W. Tobin^b, William R. Usry^a, Edgar Voelkl^a, Karsten S. Weber^a, Robert W. Owen^a

^a*nLine Corporation, 4150 Freidrich Lane, Suite A, Austin, TX 78744*

^b*Oak Ridge National Laboratory, Oak Ridge, TN 37831*

Abstract. Direct to Digital Holography (DDH) has been developed as a semiconductor wafer inspection tool and in particular as a tool for seeing defects in high aspect ratio (HAR) structures on semiconductor wafers and also for seeing partial-height defects. While the tool works very well for general wafer inspection, it has unusual capabilities for high aspect ratio inspection (HARI) and for detecting thin residual film defects (partial height defects). Inspection of HAR structures is rated as one of the highest unmet priorities of the member companies of International SEMATECH, and finding residual thin film defects (in some cases called “stringers”) is also a very difficult challenge. The capabilities that make DDH unusually sensitive include: 1) the capture of the whole wave—both the classical amplitude captured by traditional optical systems, and the phase of the wave, with phase potentially measured to $\sim 1/1000$ ’th of a wavelength or ~ 2 to 3 Angstroms for a deep ultra-violet (DUV) laser; 2) heterodyne detection—this allows it to capture very low signal levels; and 3) a head-on geometry using a collimated laser beam that allows best penetration of HAR structures. The basic features and methods of this patented technology are presented, along with simple calculations of signal strength and expected noise levels for various circumstances. Full-wave numerical calculations of electromagnetic field penetration into HAR contacts and experimental results from various wafer types and structures are also presented.

INTRODUCTION

Denis Gabor invented holography during the late 1940’s in an effort to improve the resolution of electron microscopy.¹ The invention of lasers provided a light source sufficiently coherent to make it practically useful. Also, the original invention had the complication of being “in-line” which is to say that the illumination and target beams were the same beam—i.e., they were co-linear with one another. This meant that the hologram was mixed in with the illumination beam, which was just a noise source from the point of view of the holographic wave. In the early 1960’s

Leith and Upatnieks invented optical spatially heterodyne holography.^{2,3} This form of holography used a reference beam combining with the target beam at an angle to form the hologram. When replayed the illumination beam is separated from the replayed target wave. Along with the use of lasers this made holographic recording a practical, if not convenient, reality. Recording and replaying a hologram on film or photographic plates in general required hours of patient work setting up, developing the plate in the darkroom, and then replaying the hologram. While it was possible to use this technique (typically in the form of holographic interferometry⁴) for precision scientific measurements, the difficulty and time

involved precluded its use except in the case of measurements considered important enough to justify the time and expense involved. Optical Direct to Digital holography was invented at ORNL.^{5,6} Using this invention, a true hologram is recorded digitally so that both the amplitude and phase for the original target wave are available at every recorded pixel. This technique allows measurements to be made at the camera frame rate, so that precision phase and amplitude measurements can be made with large-format digital cameras at high frame rates. Charge-coupled device (CCD) cameras with 4Mpixels and frame rates of 30 frames per second (fps) are presently available and it can be expected that larger formats and higher frame rates will become available. Since the potential measurement resolution with the phase-sensitive measurement is the order of $1/1000^{\text{th}}$ of a wavelength, a deep ultraviolet (DUV) laser allows measurements with a potential resolution of 2 or 3 Angstroms along the direction of propagation of the laser beam. With the digital technology this opens up many possible applications, including metrology and defect inspection for semiconductor process diagnostics. One immediate and important application that has been under development is the inspection of semiconductor wafers, and in particular the inspection of HAR structures and also of defects that present themselves as phase objects, where other optical inspection techniques have considerable difficulty in achieving a reasonable defect signal, or any signal at all.

BRIEF OVERVIEW OF DDH

A number of inventions were required to make it possible to capture true holograms digitally. Because of dynamic range (photo-electron well depth) requirements, CCD camera pixels are not smaller than about 7 microns, and typical pixel sizes for a full-well depth the order of 300,000 photoelectrons are 12 to 14 microns. Since classical holograms are made without a lens, the diffraction pattern from point features rapidly becomes the order of the wavelength of light being used. This means that it is impossible to capture classical sideband holograms from visible or DUV light (wavelengths from 800 nm to ~ 100 nm) with a CCD camera—the pixels are much larger than the spatial frequencies to be sampled. Additionally, the carrier frequency for classical heterodyne holograms is created by interfering the reference and target beam waves at typical angles around 30 or 45 degrees. Once again the distance between fringes is the order of $\lambda / \sin(\theta)$, which for visible or DUV light and

typical angles is less than a micron—far too small for a CCD camera to record. Beyond this problem, there is the problem of separating the target beams and reference beams as well as the twin images (real and virtual) so that the measurement produces only the phase and amplitude of the target beam. The DDH invention implements techniques to overcome all of these challenges and provide the amplitude and phase of the target beam for every pixel.

Distinguishing Features

There are a number of different features that allow the true digital acquisition of holograms.

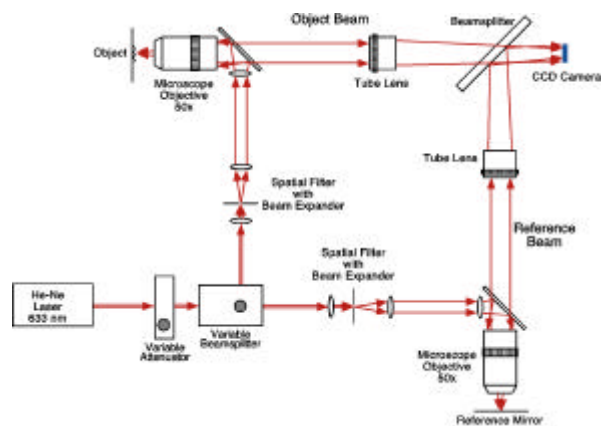


FIGURE 1. Schematic of a simple DDH system design using a HeNe laser and a Mach-Zehnder layout with through-the-lens illumination. This is schematically similar to the Fathom DUV system produced by nLine Corporation.

Multi-Megapixel CCD Cameras

While not an innovation, the availability of megapixel and larger digital cameras is required to allow analysis of usefully sized areas with suitable throughputs. Such cameras began to be reasonably available in the 1995 time-frame, and this is an enabling technology for DDH.

Focused At Camera Plane

One of the techniques required for DDH true digital holography is to focus the target image at the digital-camera recording plane. Figure 1 schematically shows a suitable geometry with the target (object) imaged on the CCD camera. This eliminates the diffraction fringes that occur in classical sideband holography due to the image being

unfocused, and is one aspect of allowing the digital camera spatial sampling to be adequate to record the hologram.

Small angle between reference and target beams

An additional technique required for adequate spatial sampling is to set up the hologram carrier frequency so that the digital camera can record it. From either Shannon's Theorem or the Nyquist limit it is obvious that there should be at least two pixels per fringe of the spatial carrier frequency in order to record it. It can be appreciated that since the distance between carrier frequency fringes is proportional to $1/\sin(\theta)$, then making theta, the angle between the reference and target beams, small is a solution. Small combining angles can lead to spatial carrier frequency fringe densities that are low enough to be resolved by the typical 12-micron pixels of a CCD camera. Typical angles for combining the two beams are less than a degree. The DDH design allows for the angle to be adjusted from zero up past the Nyquist limit (two pixels per fringe) of the CCD camera. This is again illustrated in Figure 1, where it can be seen that rotating the final "beamsplitter" (in this case used as a beam-combiner), schematically shown before the CCD camera, can introduce angles from zero degrees and up. In fact, only a degree or two of rotation will produce carrier frequencies beyond the Nyquist limit of the CCD camera.

Magnification To Resolution

In addition to having at least two pixels per fringe to record the hologram, it is also necessary to have at least two carrier frequency fringes, and possibly three, across the spatial resolution (Rayleigh resolution or line-space pair resolution) of the optics imaging the target on to the CCD camera. This is discussed in the first paper by Leith and Upatnieks² and in more detail in Ref. 7, and can be interpreted in at least two ways. The first interpretation is that this is the angle required to keep the spatial frequencies in the hologram from mixing with the undiffracted beam when the hologram is replayed (i.e., produce an angle large enough in the replay to separate the hologram from the zero order or replay beam). A second and equivalent interpretation is that this is the carrier frequency required to separate the hologram (sideband) from the zero-order beam (autocorrelation) in Fourier space. For uncorrelated objects (objects which do not have any significant signal in the autocorrelation beyond the nominal image spatial bandwidth) the zero order beam has an autocorrelation bandwidth in Fourier space just equal

to the bandwidth of the object passed by the lens. For highly correlated (repetitive) objects the autocorrelation bandwidth is equal to twice the object bandwidth, and it is necessary to place three carrier frequency fringes (three line-space pairs) across the spatial resolution of the optics in the CCD plane in order to separate the hologram sideband from the autocorrelation (carrier frequency must be three times the image bandwidth). What this means is that the target must be magnified enough so that there are a minimum of four CCD pixels (two carrier frequency fringes) across the spatial resolution of the optics in the image plane, or for highly correlated objects, at least six CCD pixels (three carrier frequency fringes). The carrier frequency fringe density and magnification are independently controlled by the beam-combiner angle and the magnification of the optics. The beam-combiner angle can be controlled in real-time, but for precision diffraction-limited optics the magnification of a particular objective lens is usually fixed, so the relationship of the magnification to the spatial resolution must be included in the design of the optics.

Fourier Transform Analysis

Rather than going through the complex derivation for the use of Fast Fourier Transform (FFT) analysis to separate the target beam and object beams, graphical examples will be presented. See Ref. 7 for more details.

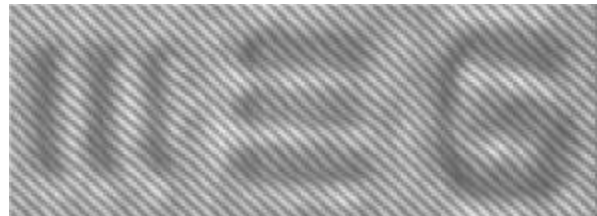


FIGURE 2. Section of a raw hologram of a chrome on chrome Air Force Resolution Target.

Figure 2 above is a section of a raw hologram showing the raw carrier frequency fringes from the reference and target beams interfering as modulated by the target. This digitally recorded hologram records amplitude and phase the same way that all heterodyne holograms do. Amplitude of the target wave is recorded by the fringe contrast—as the target beam amplitude changes the fringe contrast darkens or brightens. The actual spatial motion of the fringes records phase. As distance or index of refraction of the target changes the phase of the wave changes causing a modulation of the carrier frequency fringes, and the fringes move away from being perfectly linear

and move up or down depending on whether phase is increasing or decreasing. For a well-designed DDH system the carrier frequency fringes are very linear and evenly spaced, only modulated by the target object height changes or index of refraction changes. The carrier frequency is represented by a single point in Fourier space, since it is effectively just a plane wave in this case. To the extent that there is some curvature or variation from linear spacing of the fringes when a perfectly flat object is made into a hologram, the system can be “flat-field corrected” to remove both the phase variation and any amplitude variation, by dividing the complex image of whatever is the target by a complex image of a perfectly flat object, where the same optical conditions and image processing are used for the “flat-field” object hologram as for the hologram being corrected.

In order to have good FFT analysis of digital holograms the carrier frequency needs to be linear over a megapixel hologram within one or two waves (one or two carrier frequency fringes). Otherwise the carrier frequency becomes spread out over many frequencies (cannot be identified by a single frequency), and analysis of the holograms becomes much more difficult.

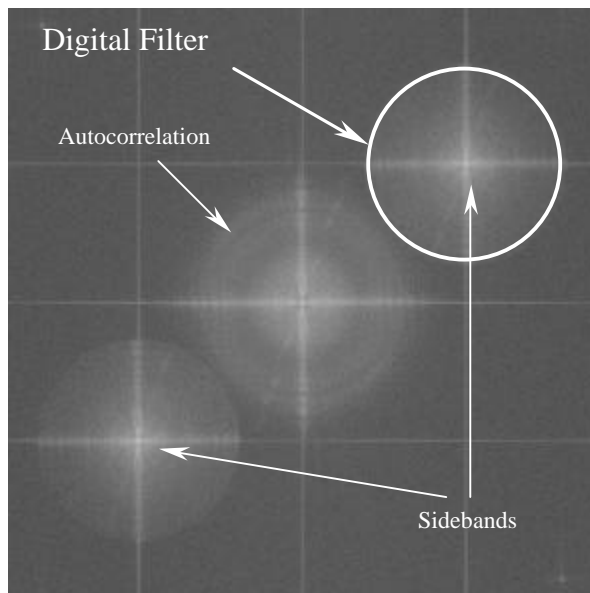


FIGURE 3. This is the FFT of the complete hologram partially shown in Figure 2. The log of the frequency amplitudes are plotted as a gray-scale against x, y coordinate.

The basic features of FFT analysis of digital holograms can be seen in Figure 3. Zero frequency for both x frequencies and y frequencies is in the center of the figure. The horizontal axis is for x frequencies and

the vertical axis is for y frequencies. A CCD camera records light intensity, which is electric field squared. The hologram electric field is the sum of the target and reference electric fields, $E_H = E_R + E_T$. Thus the circular pattern in the center is the FFT of the reference beam electric field squared plus the target beam electric field squared (autocorrelation—the FFT of a square in real space is the autocorrelation in Fourier space). The sideband in the top right quadrant is the FFT of the target beam electric field times the reference beam electric field complex conjugate, and vice-versa for the sideband in the lower left quadrant. Since the reference wave is effectively a plane wave, a single point in Fourier space represents it, which is the brightest spot or carrier frequency in each of the sidebands. The strong vertical and horizontal lines in the FFT, at the figure center and coming from each of the sidebands, are due to differences in intensity at the pixel edges of the CCD (due to variation of the image), which since they represent square waves contain all frequencies resolvable by the CCD camera. The target beam phase and amplitude are recovered from the FFT by translating the FFT zero-zero axis to the carrier frequency of one of the sidebands, and applying a smooth digital low-pass filter (e.g., Hanning window or Butterworth filter) so that everything outside the target wave sideband is zeroed out. When the inverse FFT of this centered and filtered sideband is taken, phase and amplitude images can be constructed from the resulting complex image. Figure 4 is the resulting 3D phase image from inverting the sideband of the FFT of the section of hologram shown in Figure 2.



FIGURE 4. The 3D image above is produced by taking the FFT of Figure 2, translating the zero-zero axis to the sideband carrier, applying a digital filter and taking the inverse FFT and the phase of the resulting complex image is used to produce the true 3D image (height plus x-y dimensions).

Advantages For HARI And Phase Objects

The DDH technology has some unique advantages for High Aspect Ratio Inspection and an obvious advantage for phase objects. In particular for HARI work:

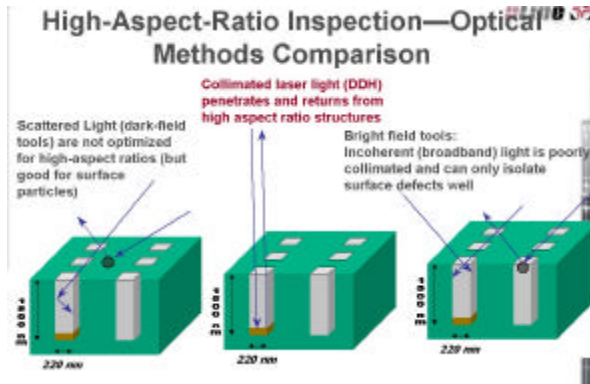


FIGURE 5. Comparison of HAR structure penetration by optical methods. Light-scattering and incoherent light penetrate high aspect ratio structures poorly compared to a collimated laser beam.

1. The head-on geometry with a collimated laser beam (Gaussian beam waist) at the wafer surface has the best chance of penetrating HAR structures. This is demonstrated graphically in Fig. 5 and the head-on geometry schematically in Fig. 1. Light-scattering by definition enters or leaves at an angle, which makes it unsuitable for HAR penetration. Similarly, incoherent light can only be collimated over very short distances, again making it incompatible with penetration of HAR structures.
2. Because the technology is spatially heterodyne (has a spatial carrier frequency) with the power in the hologram proportional to reference beam electric field multiplied by target beam electric field with the reference wave supplying much of the power, the DDH technology is sensitive compared to classical amplitude measurements. For instance, a 10% electric field return would be a 1% signal (electric field squared) for a classical bright-field or light-scattering tool, but is a 10% signal for the spatially heterodyne DDH tool.
3. In addition to being spatially heterodyne, the DDH technology is phase sensitive, with the typical photon noise-limited phase resolution being as small as one-thousandth of a wavelength. This gives an additional level of sensitivity to DDH measurements, because of the very high sensitivity of the phase measurement.
4. Relatively low incident energy: the fact that it is both spatially heterodyne and phase sensitive allows a DDH tool to inspect with relatively low energy levels. For instance, only the order of four microjoules would be required to expose the wafer field of view (fov) of a 4 Mpixel CCD camera using a 248 or 266 nm DUV laser, assuming a relatively poor 10% reflectance from the wafer and a high efficiency camera, and throwing away half the target illumination light in the beam-combiner (note that Si or SiO₂ on Si is nominally 70 to 80% reflective at, for instance, 266 nm).

For inspection of phase sensitive objects (e.g., very thin layers of oxide or other material left after an etch—“stringers”), a tool that measures phase is

required. Either brightfield or darkfield amplitude tools have a very hard time seeing these defects because they look exactly like their surroundings (the amplitude reflection is extremely similar or identical to the material around them). However, a tool using the DDH phase-sensitive technology sees these defects easily, since they can return a very different phase signal due to either their thickness or their optical properties, even though the amplitude signal is changed little or not at all.

SIGNAL CALCULATIONS

The expected return signal from coherent light incident on sub-wavelength HAR structures is a difficult calculation, both because the structures are sub-wavelength and because they are high aspect ratio. Simple estimates of the return signal can be made using just ray-tracing height analysis and assuming no phase-change on reflection or change of index of refraction and combining this with diffraction estimates. More sophisticated estimates can be made by using an exact one-dimensional (1D) version of Maxwell’s equations—the transmission-line equations (see, e.g., Ramo, Whinnery, and Van Duzer⁸), along with the full optical properties of a materials stack and adding simple diffraction estimates. Estimates of the penetration of HAR contacts have been made using a full-wave 3D electromagnetic finite-element boundary value numerical calculation and will be discussed below. The most sophisticated analysis uses a full-wave vectorial finite-difference time-domain numerical solution, where some initial work has been done for the DDH problem and codes are available to address these types of structures on wafers. Solvers that do not account for all penetrable (by DUV radiation) surfaces and the optical properties of all materials involved along with the sub-wavelength geometry are not suitable for addressing the exact numerical solution of this class of problems.

Simple Phase Estimates

Simple estimates of phase signal strength can be made by just using known indexes of refraction and geometrical heights to calculate the expected phase change. For instance, for 50 nm of SiO₂ left at the bottom of a 1 micron deep contact in the oxide, and neglecting first-surface reflections and phase change on reflection from different materials, the expected phase difference for a wave penetrating the “bad” contact (contact with oxide at the bottom) as compared

to a wave penetrating a good contact (no oxide at the bottom) is just the phase change due to a double pass through the oxide (once going in, once returning) minus the phase change due to a double-pass through the equivalent depth of air. So the net difference in phase signal is given by:

$$\Delta\phi = 2(n_1l - n_2l) / \lambda \quad (1).$$

Where n_1 is the index of refraction of SiO₂ at the DUV wavelength, n_2 is the index of refraction of air at the DUV wavelength, l is the path length over which the material difference occurs (air vs. SiO₂) and λ is the DUV wavelength. For 266 nm, the index of refraction of SiO₂ is ~1.5 and the index of refraction of air is ~1.0, so that the expected phase change, $\Delta\phi$, for the 50 nm path length is 0.38 waves, or more than 100 times the expected noise level for photon statistics. This only holds if the transverse dimensions of the defect (contact in this case) are larger than the Rayleigh resolution of the lens, otherwise this signal must be corrected for diffraction. For equations to make simple estimates of the phase change on reflection or differences in the phase change on reflection for different optical materials, see the TL equations below, or see the paper by Church and Lange⁹.

Simple Diffraction Corrected Phase Signal

For sub-resolution objects, the phase signal can be estimated by spreading it out over the resolution of the imaging optics. Coherent electric fields add in a vectorial fashion, of course, so the electric field signal from the sub-resolution object adds with the electric field from the surroundings. Since the intent is to subtract similar areas from neighboring die to find differences, without loss of generality the neighboring objects can be assumed to just be a reflective plane (when two die are subtracted, to the extent that they are similar the neighboring objects drop out on subtraction, leaving only the difference). The phase signal can be assumed to spread just as the amplitude due to the vector addition of the electric fields, so a simple estimate of the signal from a sub-resolution target or defect can be found by just spreading the “phase volume” of the defect out over the area of the Rayleigh resolution of the imaging optics. The Rayleigh resolution is the distance from the peak to the first zero of the Airy function for a point being imaged by a diffraction limited lens, and is given by (for on-axis illumination with coherent illumination):

$$\delta R = \lambda / NA \quad (2)$$

where λ is again the laser illumination wavelength and NA is the numerical aperture of the imaging optics. Again for a 266 nm DUV laser and for instance a 0.5NA objective, the phase signal is spread out over an area of the Rayleigh resolution squared. Given once again a 50 nm layer that is for instance 200 nm diameter, the expected phase volume is (200 nm)² times the 0.38 waves already calculated. Dividing by the Rayleigh resolution squared gives the desired simple estimate of the phase signal from this defective contact, when spread out by diffraction, as 0.054 waves, still more than an order of magnitude larger than the theoretical photon statistics noise level. It will be shown below that the signal can actually be much larger than this due to index of refraction differences of materials.

Exact 1-D Signal Calculations— Transmission Line Equations

As already mentioned above, the transmission-line (TL) equations are an exact solution of Maxwell’s equations in one dimension. As such, they are very useful for calculating the exact reflection, including multiple surfaces and phase, for normally incident waves on materials stacks on wafers. The interested reader is referred again to Ramo, Whinnery, and Van Duzer⁸ for discussion of calculating the reflected voltage given load impedances, and calculation of the load impedance for a particular material and thickness given its electrical properties. In order to use the TL equations to solve for reflected electric field, V (voltage) is replaced by E (electric field), I (current) is replaced by H (magnetic induction), transmission line capacitance per unit length is replaced by the dielectric constant ϵ of the medium, and transmission line inductance per unit length is replaced by the magnetic permeability μ of the material. The only fly in the ointment here is calculating the dielectric constant from the commonly given/measured optical properties of semiconductor material, n (index of refraction) and k (extinction coefficient). For instance, the “capacitance” and “inductance” to be used in the TL equations for material X can be calculated from (see Born and Wolf¹⁰ for calculation of the dielectric constants from n and k):

$$C_X = \epsilon_X = \epsilon_0(\epsilon_1 - i\epsilon_2) \quad (3)$$

$$\epsilon_1 = n_X^2(1 - k_X) \quad (4)$$

$$\varepsilon_2 = 2k_X \quad (5)$$

$$L_X = \mu_0 \quad (6)$$

where C_X is the capacitance of material X to use in the impedance calculation, L_X is the inductance of material X (assumed to be non-magnetic), ε_0 is the dielectric constant of free space, μ_0 is the magnetic permeability of free space, and n_X and k_X are the index of refraction and dimensionless extinction coefficient (the commonly quoted optical n and k) of material X. Armed with the capacitance and inductance and material thickness, the impedance is immediately calculated and the amplitude and phase of the reflected wave are calculated from:

$$V_o = V_i \frac{(Z_L - Z_0)}{(Z_L + Z_0)} \quad (7)$$

where V_o is the reflected electric field at the location just above layer X, V_i is the incident electric field just above layer X, Z_0 is the characteristic impedance of the material just above layer X and Z_L is the load impedance of layer X, given its thickness, characteristic impedance, and the impedance beneath it. The layer furthest down in the stack is assumed to have no second surface reflection, so that its impedance is just the characteristic impedance of that material (thickness is assumed effectively infinite—appropriate for materials that absorb everything not reflected that enters the material—e.g., Si at 266 nm), and the impedance of the entire stack can be built up one layer at a time.

The exact reflected electric field can thus be calculated for complicated materials stacks and can be expected to be correct for the center of large (large compared to the wavelength) areas, including reflections from all surfaces and changes of phase at all surfaces.

Returning to the example of calculating the signal from 50 nm of oxide at the bottom of a contact vs. a contact with only Si at the bottom, the calculated phase difference is 0.71 waves using the TL equations rather than the 0.38 waves calculated from the simple phase model discussed earlier. So there is almost a factor of two more signal due to the materials properties when the exact TL equations are used.

A more complex example of using the TL equations to calculate the expected signal is shown in Fig. 6. In this example the theoretically predicted return signal from the wafer, calculated using the 1D

TL equations is compared to the actual measured signals. The wafer is an International SEMATECH supplied contact wafer with 250 nm design rules. It can be seen that the TL equations are qualitatively very good, but apparently miss the actual transverse dimensions by quite a bit, as would be expected for 1D (z-dimension) equations when the transverse features become the order of or smaller than the wavelength of light.

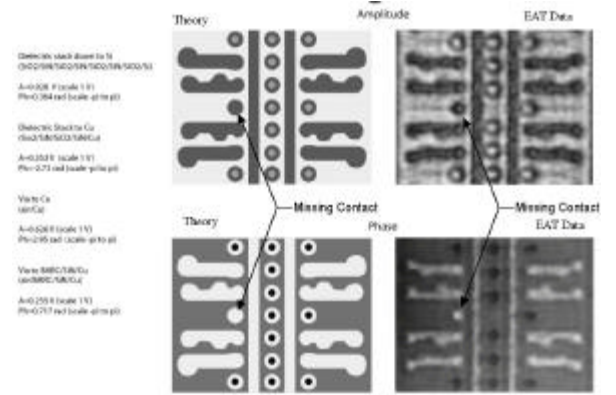


FIGURE 6. Comparison of 1D TL theory with actual experimental measurements from the Fathom DDH tool. Top left is the theoretically predicted amplitude for one of the International SEMATECH IDA Contact wafers, and top right is the measured amplitude (electric field). Bottom left is the theoretically predicted phase and bottom right is the actual measured phase. The TL equations theoretically predicted signal for the various material stacks (incident field 1, incident phase 0 degrees) is printed to the left. Materials in the stack for the images shown include Si, SiN, SiO₂, and Cu.

Combining Diffraction and TL Equations

Just as for the simple phase equations, simple estimates of diffraction can be combined with the TL equations to estimate the signal. Using the same example of a 0.5NA objective, the expected signal after diffraction becomes almost a factor of two larger when the TL equations are used to estimate the phase change. The effect of diffraction is modeled identically in both cases. It is worth noting in passing that the TL equations also give the correct value for the expected electric field amplitude, so both quantities are correctly modeled with the TL equations, whereas the simple phase model does not provide the amplitude at all. For the example cited, the TL equations predicted electric field amplitude difference between the defective and non-defective contact, not including diffraction, is about 0.04 where the incident electric field is taken to be 1.0.

Penetration Of EM Waves Into Contacts Or Vias In Dielectrics—Full Wave 3-D Boundary Value Numerical Solutions

Penetration of electromagnetic (EM) waves into metallic structures is well understood--any feature less than a half-wavelength is cutoff for rectangular structures (the wave does not penetrate), and less than ~ 0.7 wavelength is cutoff for cylindrical metallic structures. This applies to a collimated laser beam just as it does to all EM waves. Penetration of EM waves into contact holes in a dielectric is more difficult to understand since the wave propagates in the dielectric and “leaks” out of the contact (neglecting any possible sub-wavelength effects, nothing can come back into the contact because of total internal reflection from the dielectric side). Additionally, the problem is not a “far-field” problem since the depth of the contacts is only a few wavelengths. The far-field approximations often used to study propagation in “leaky” dielectrics are not applicable (see, e.g., Yariv¹¹).

Lee Berry and John Whitson at Oak Ridge National Laboratory developed a 3-D full-wave numerical electromagnetic code for radio-frequency (RF) plasma reactor studies. The code was modified by one of the authors (CET) to study laser penetration into sub-wavelength HAR structures. The EM fields can have 3-D structure, but the geometry (excluding sources) is assumed to have one symmetry dimension (the radial dimension in the case of a contact). The code is a finite difference boundary-value solver using a component of the potential of E and of the potential of B in the directions with spatial variation. Spatial variations due to source currents in the ignorable dimension are resolved into independent Fourier modes.

Typical results of applying this code to the study of contacts in dielectric are shown in Fig. 7. Due to memory limitations (at the time the calculation was made only 2 gigabytes of virtual memory were available), it was necessary to limit the input boundary to nine wavelengths (only part of the input boundary is shown in the figure) and limit the z-dimension (direction of propagation) calculation to 12 wavelengths of useful calculation. Typical features of boundary-value code solutions are shown by this calculation. The small apparent “ridge” in the electric field at the center of the contact is an artifact produced by the finite boundary effect for the input wave (a much longer input boundary should remove this). With a boundary-value code, finding the reflected field is difficult, since the code calculates the sum of all fields propagating in all directions given the imposed boundary values. To avoid this problem an absorptive

boundary condition was used in the far z-dimension. This addition of absorption changes the material impedance where the absorption is added and causes some reflection of the wave, which can be seen as the standing wave pattern in the solution for the y-value of the electric field. The actual value of the inward-propagating electric field is calculated from the standing-wave ratio at 12 wavelengths, and is found to be 64% of the electric field strength at the entrance to the contact. This would be the signal actually predicted to be seen by a DDH tool, but the signal seen by a classical amplitude tool would be the square of the electric field, or $\sim 41\%$ of the input power. It can be seen that the field is indeed “leaking” out, but slowly for the present purposes. The calculation of the field at 12 wavelengths for a quarter-wavelength contact corresponds to the wave penetrating an aspect ratio of 12, both going in and returning to the surface.

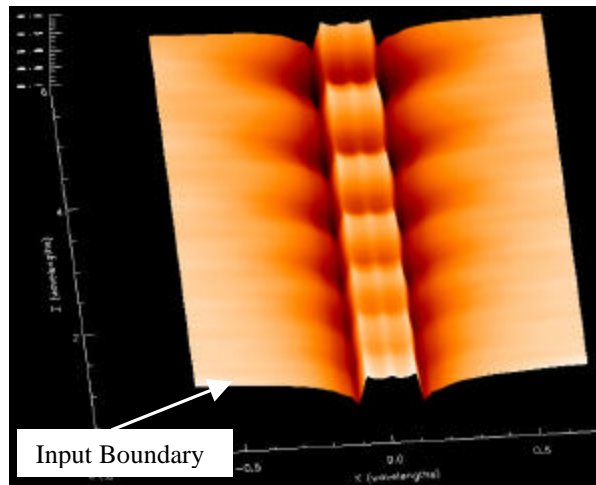


FIGURE 7. Full-wave 3D numerical solution for a nine wavelength boundary “plane wave” launched into a quarter-wavelength cylindrical hole (contact) in dielectric. The solution for the y-direction (radial) electric field is plotted vs. penetration distance z, in wavelengths, into the contact and vs. the radial dimension x of the contact. The solution exhibits a standing wave due to an absorptive end boundary condition. The propagating field at 6 wavelengths (aspect ratio of 12, in and back out) is $\sim 64\%$ of the entrance field.

Full Wave 3-D Finite Difference Time Domain Solutions

Other 3D numerical codes are available for analysis of these kinds of difficult problems. One example is the finite difference time domain code TEMPEST developed at Berkeley for semiconductor wafer lithography simulations and 3D scattering

simulations.^{12,13} Since this code propagates the wave in the time domain, reflections become much easier to deal with and it is possible to separate incoming and outgoing propagating waves. Also, the code was designed for semiconductor lithography, which gives it an excellent start on being useful for studying coherent reflections from wafer geometries. The code has also been developed for commercial use as part of a suite of tools for lithography simulation by Panoramic Technologies.¹⁴ Some very preliminary work has been done for nLine Corporation using the Panoramic Technologies suite. Figure 8 shows the electric field intensity resulting from a plane wave incident on a particle. The calculated field compares favorably with the measured field pattern published for an atomic force microscope (AFM) and scanning near-field optical microscopy measurement.¹⁵

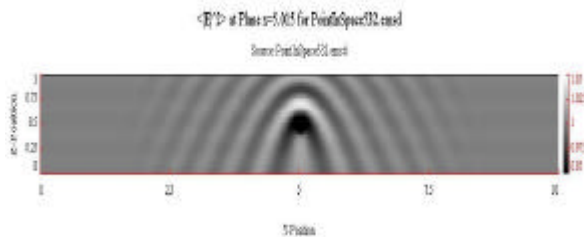


FIGURE 8. Electric field intensity due to scattering from a particle as simulated by the Panoramic Technologies EM Suite. The vertical and horizontal distance scales are in microns (1 micron vertical, 10 microns horizontal) and the gray-scale for the electric field is relative to an incident intensity of 1.0, and varies from 0.95 to 1.05 with the particle as the black spot in the center.

NOISE SOURCES AND ESTIMATES

Discussion Of Noise Sources

Anything that is involved in producing the laser beam, propagating the beam, reflecting the beam, imaging the beam, capturing the image digitally or computing the amplitude and phase or amplitude and phase differences from the digitally captured hologram is a potential source of noise, including all the optics and mechanical systems associated with the optics, stage, vacuum chuck, or wafer. Some sources of noise are more important than others, and even if all these sources of noise are zero, there is still a fundamental photon counting statistics noise limit due to the dynamic range of the sensor and the finite power of the laser. Various possible noise sources are discussed below and quantified where reasonable.

Back-Reflections And Ghosts

One very strong known source of noise for coherent laser illumination is reflections from the optics that propagate back to the CCD camera and interfere with the signal beam or the reference beam. If perfect anti-reflection (AR) coatings could be manufactured then the optical noise due to reflection interference could be driven to zero. Such perfect coating technology is not available, but extremely good coatings are available and coatings with measured reflectances less than 0.01% for 266.1 nm normally incident light have been produced for nLine Corporation. Figure 9 below shows a sample measurement from just such an AR coating on fused silica.

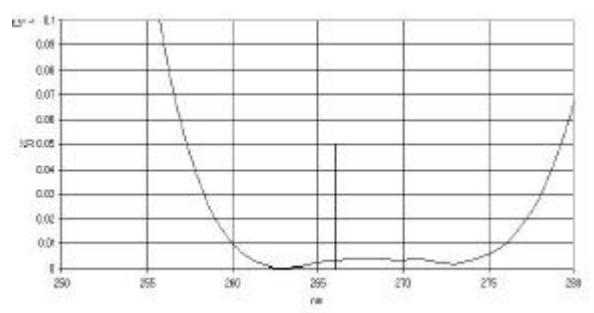


FIGURE 9. Sample measurement of an AR coating on fused silica, which has less than 0.01% reflectance at 266.1 nm for a normally incident wave.

Even with an absolute state of the art AR coating, the predicted noise due to a direct back-reflection (reflection from a single surface which propagates back to the CCD camera) can be significant. Assuming that the back-reflection covers about the same area as the original image (could be focused or expanded, there is some design control over this) then the predicted phase-noise level due to a single reflection from a 0.01% AR (10^{-4}) coating is about 1% (10^{-2}) of a wavelength, and can have this kind of effect on the carrier fringe intensity, distorting it by the amount of the electric field. This is because the hologram is recorded as the electric field and the noise electric field strength is proportional to the square root of the reflected noise intensity. If through-the-lens illumination is used, then there can be as many as 12 to 20 surfaces reflecting directly back to the CCD camera, so that noise levels become too high. This back-reflection noise can be reduced another factor of 100 to 1000 by using a polarizing-beam-splitter (PBS) to reflect the beam into the objective and designing the objective with a quarter-wave plate as its last optical element.⁶ This can theoretically reduce the back-reflections another two to three orders of magnitude,

so that the back-reflection noise level theoretically drops below the photon statistics noise level. Ghost reflections can then become a dominant noise source.

Ghosts are multiply reflected beams (from two or more optical surfaces, e.g., first and second surface of a lens) that propagate back to the image plane (CCD camera). Since such a beam has reflected from two or more AR coated surfaces, its intensity could be down eight orders of magnitude (for a 0.01% reflective AR coating). Thus careful optical design and extremely good optical coatings can also be used to put the noise level from ghosts below the photon statistics noise level. It is however very important to insure that the AR coatings meet the required specification and that there are no ghosts focused so tightly as to exceed the allowable noise level.

Vibrations

Vibrations are one of the worst enemies of holography. It is easy to calculate that an optical path vibrational change of 1/8'th of a wave during the exposure will wash out the carrier frequency fringes by 30% (the fringe contrast drops to 70% of its original value) which considerably increases the noise in a hologram. This drop in fringe contrast can be understood by just considering a cosine fringe pattern (intensity due to interfering plane waves, $a^2 + b^2 + 2ab \cos(\theta)$): if the pattern moves 1/8'th wave, then the peak intensity moves over the 0.707 intensity point and the 0.293 intensity point moves over the zero-intensity point. The average peak value becomes 0.85 and the average minimum value becomes 0.15. Calculating the fringe contrast as $(I_{max} - I_{min}) / (I_{max} + I_{min})$ immediately results in a (with vibration) fringe contrast of 70% of the contrast without the 1/8'th wave vibration. Much more motion than this will totally ruin the hologram. A quarter-wave optical path change due to vibration drives the contrast to 50%, and a half-wave of vibration drops it to zero. Stiff, well-damped optical and mechanical designs can resolve this problem, along with short exposures of the camera. A nominal rule of thumb is to require that vibrational movement of the optical path during the camera exposure be less than 1/10'th wave.

Another way that vibrations can induce noise is to change the beam pointing from shot to shot. This can create wedge or bowl between the holograms being differenced. The amount of wedge or bowl is dependent on the details of the optics and the amount of the pointing motion.

Image Registration And Interpolation

If the complex holographic images are not well aligned when they are differenced then the difference will have noise in it due to the misregistration. Sources of alignment error include stage resolution and accuracy, accuracy of the original reticle and stepper shooting the die, and any possible angular variation of one die to another. In order to accurately subtract two images, they generally need to be aligned to one another in software to eliminate the noise due to misregistration. This is typically done to an accuracy of about 1/10'th of a pixel. Thus the phase noise along a long edge (an edge whose length is longer than the Rayleigh resolution of the imaging optics) can be estimated as:

$$\Delta\phi_r = 2[n_1 h (PS) PR] / (\lambda \delta R) = 2NA[n_1 h (PS) PR] / \lambda^2 \quad (8)$$

Where n_1 is the index of refraction of the line edge material, h is the height (or depth into the wafer) of the line, PS is the pixel size in object space (assuming square pixels, the linear dimension along one edge of the pixel divided by the magnification of the imaging optics), PR is the fractional pixel resolution of the software registration and interpolation, λ is the illumination wavelength as before and the other symbols are previously defined.

Noting that as discussed above there is a requirement for six pixels across the Rayleigh resolution:

$$PS = \delta R / 6 \quad (9)$$

Then the expression for the noise becomes:

$$\Delta\phi_r = (n_1 h PR) / (6\lambda) \quad (10)$$

The factor of two due to the illumination optical wave penetrating and returning from the line (traversing it twice) is dropped since the same applies to defects, so the phase noise can be considered as the noise equivalent to a defect height spread over the optical resolution. It's interesting that the noise becomes dependent only on the registration accuracy and the line height, assuming equivalent indexes of refraction for any defect and the background material. For a 500 nm line height the height of a defect equivalent to the noise would be 1.25 nm, if the index of refraction is 1.5 and using 1/10'th pixel for the registration accuracy, and converting phase to height using the 266 nm wavelength. For features with edge lengths shorter than the Rayleigh resolution, the phase noise due to

registration and interpolation is even less than calculated above.

Stray Light

In order for coherent interference from the forward scattered stray light due to optical surface roughness to be less than the photon noise, the scattering should be less than about 10^{-5} of the incident power, for all surfaces. Assuming something on the order of 100 optical surfaces from the laser to the camera, and also assuming that the associated solid angles tends to favor only those near the camera, then the scattered power needs to be about 10^{-5} of the incident power for any optical surface, particularly those near the camera or imaged at larger NA on the camera. Using the total integrated scattering formula from Stover¹⁶, this requires a nominal surface roughness of less than 6 Angstroms for the optical components for high-frequency roughness (note that this is not the same as the scratch and dig specification). This is perhaps an unnecessarily stringent specification, since the forward scattered light is basically in phase with the main beam for small surface roughness (surface roughness much less than the wavelength). For surface roughness the order of 1 nm (typical of high quality optical coatings), a relaxed specification would be to require that the noise due to the surface roughness and the vectorial addition to the phase due to the beam intensity be less than the photon noise. Since surface roughness of one or two nanometers is expected, the noise at 0.1% illumination due to the scattering would be about 0.008% of a wavelength or more than an order of magnitude smaller than the noise due to photon statistics (to be discussed below). For practical purposes, forward scattered stray light from high-quality polished optics and coatings can be ignored.

Another source of stray light is clipping on metal surfaces where the light is scattered, typically more than once for good design, before it gets back to the camera. In this case the light, having scattered from a rough surface (an unpolished machined metal surface), will nominally be arriving at all phases so that it is incoherent with the primary illumination. In this case it is desirable to design the system so that the amplitude from the scattered light is less than the photon statistics from the weakest part of the target beam (which might only be 10% to 1% of the highest target intensity at the camera). For an average of 100,000 photons per pixel in the target beam, this would imply that the stray light from clipping actually reaching the camera would be less than 0.1% of the incident beam. This is probably too stringent for incoherent light reaching the camera, but serves as a

reasonable design goal. A softer design goal would be to have the statistical noise from the clipped stray light be less than the statistical noise from the weakest part of the target beam. If the dynamic range of the target signal is 100, this would imply that the stray light reaching the camera should be less than 1% of the average target beam intensity.

Camera Noise Sources

Noise sources due to the camera electronics can also impact the signal. Some of these are discussed below.

Electronic Noise

A typical specification for the electronic noise from a high-quality CCD camera is about 30 electrons of readout noise and about 0.2 electrons per ms of dark current per pixel.¹⁷ For short exposure times (typically ~2 ms) and for intensities greater than 900 photoelectrons per pixel (typical intensities are ~100,000 photoelectrons per pixel, typical full-well-intensity for linear exposure is 300,000 photoelectrons per pixel) the camera electronics noise is negligible compared to the photon statistics, which for the example given of 100,000 average photoelectrons would be a noise level of ~300 photoelectrons (square root of the average number of photoelectrons).

Camera Nonlinearities

Nonlinearities in the camera response can cause higher harmonics of the sideband to appear. These harmonics appear at higher brightness (camera exposure) and can typically be positioned so that they do not interfere with the hologram sideband. Additionally, the DDH tool can be operated at a level where the higher harmonics (fourth and above) do not appear. The harmonics can be experimentally identified by looking at the live FFT of the hologram of a bare wafer or good mirror at a low spatial carrier frequency (since there is no content in the hologram the sideband and autocorrelation don't visibly overlap). As the camera exposure or laser intensity is increased the second and then the third and etc. harmonics will appear and can be identified. As the sideband position is changed (by varying the beam-combiner angle) the movement of the harmonics can be watched and the position of each harmonic identified, and the level it appears at associated with the hologram brightness. Figure 10 shows an example of a bare wafer hologram with a brightness high

enough that the third harmonic just begins to show, but with the third harmonic far from the sideband's frequency aperture. Peak brightness in the original hologram was about 1800 bits out of 4096 bits (not quite a 50% exposure).

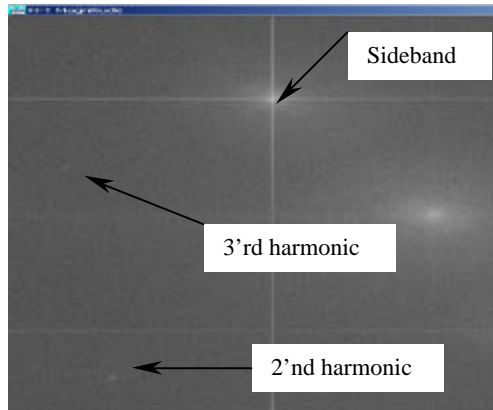


FIGURE 10. Fourier transform of a bare-wafer hologram showing the dim second-harmonic and the very dim third-harmonic. Note that the FFT is on a log scale, so they are even dimmer than they appear.

Gain Variation

Variation in gain from pixel to pixel can cause the hologram fringes to change their apparent position—this is a source of noise when subtracting complex images which have different average brightness (even though they are DC normalized), or if the image must be registered significantly in software to match it up with the next image. To first order, flat-field correction removes this noise source. To a higher order, gain-mapping the pixels in the camera and correcting them for gain before processing the hologram can equalize the pixel to pixel gain and remove this noise source below the level of measurability, if it is measurable to start with. Subtracting bare wafer or bare mirror holograms from one another at varying brightness (exposure) levels (with the DC variation normalized out) can reveal the presence of any noise due to gain variation, that exceeds the other noise sources. Subtraction of static holograms from a bare wafer or flat mirror (taken at different times only, all other parameters held constant) will reveal the static noise level of the system to compare with the exposure-varied noise.

Camera MTF

The camera modulation transfer function (MTF) can alter the fringe contrast of the hologram carrier-

frequency fringes. Typical uncoated CCD camera specifications for MTF at Nyquist (two pixels per fringe) are 65%.¹⁷ With a UV sensitive coating on the CCD, typical fringe contrasts achieved at nLine corporation are 40% to 50%, depending on the carrier frequency, with the order of 2.7 pixels per fringe. This is considerably less than the minimum quoted CCD MTF, and is attributed at least partially to the presence of the UV-sensitive coating on the CCD sensor. The effect of fringe contrast on noise will be discussed below in the photon statistics section.

Optical Imperfections

Dust on the optics, scratches or digs in the optical surfaces, or imperfections internal to the fused-silica or quartz for the transmissive optics can cause noise in the complex difference images if the original images are not flat-field corrected. This occurs because the noise is always in the same location, so registering the images moves the noise in one image relative to the other. Flat-field correction removes this noise to a considerable extent, but the dynamic range of the image at the optical defect location is at least reduced by the amount of the defect signal. The best way to avoid this is not to have any imperfections in the optics. Second-best is to use the flat-field correction (nominally always required unless it is known that the images to be subtracted are perfectly registered in hardware).

Figure 11 shows an example of the phase from a hologram without flat-field correction. There is an optical defect visible in the image, and also a true defect on the wafer. Figure 12 shows the same phase image after flat-field correction. The optical defect is no longer visible, but the wafer defect and wafer features remain, and the image appearance is visibly improved.

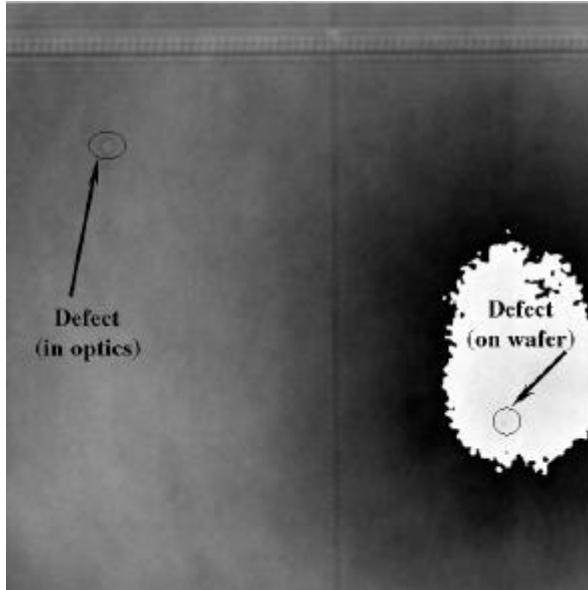


FIGURE 11. Phase image with no flat-field correction containing both an optical imperfection defect and a true defect on the wafer. The bright white area is a phase jump, which normalizes out of the image as seen in the next figure.

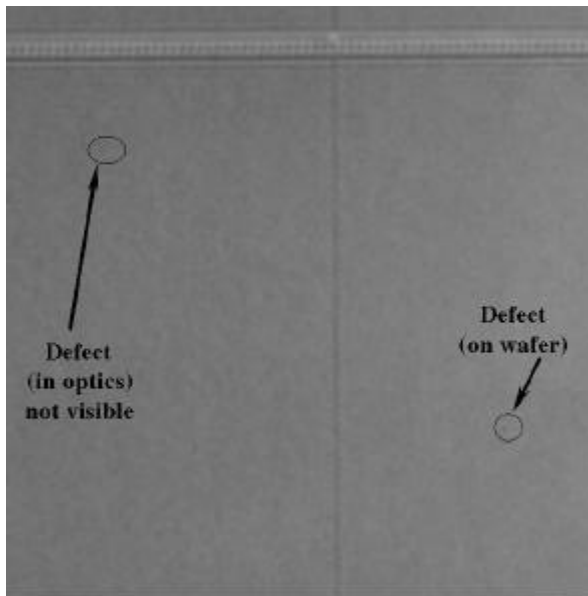


FIGURE 12. Phase image after flat-field correction. The correction removed all visible traces of the defect in the optics without affecting the wafer features, and greatly improved the visual quality of the image. Note that the phase jump in the previous figure was also normalized out with the flat-field correction.

Laser Noise

Pointing

Slow changes in laser pointing (1 or 2 seconds) can have the same effect as slow vibrations of the optics. While the holograms are still good (high-contrast carrier frequency fringes are formed) the pointing change can introduce wedge or bowl in the hologram difference images, and other possible differences in the images due to change of direction of the illumination. The amount is hard to quantify since it is dependent on the details of the optical design. This can be measured however using tools such as a wavefront sensor. Such an instrument is available with a Shack-Hartmann sensor¹⁸ and can be used to quantify the pointing error of the system. Holographic difference images made by looking at the same spot on a bare wafer or mirror but subtracting images separated in time can also help to quantify the system pointing error (by looking at wedge or bowl across the phase image), but give little information about where the error occurs.

Intensity and Phase Noise

Typical laser intensity fluctuations from hologram to hologram on the DDH tool are less than 1%. Any DC fluctuation (fluctuation by a constant across the entire beam) can be normalized out, as can any DC fluctuation in the phase. Since the laser is single-mode both longitudinally and transverse, fluctuations in the mode structure are expected to be dominated by photon statistics. It is however known that the high-Q DUV cavity is sensitive to vibrations, so the laser output must be monitored in order to discard any frames where the beam variation exceeds the 1% standard.

Process Variation

Differences in reaction rates, concentrations, geometry, temperature across the wafer, acceleration due to spin, machine variations, etc. can cause die-to-die differences during fabrication of a semiconductor wafer. These differences are commonly known as “process variation” and are generally ignored if they don’t affect the performance or longevity of the resulting chips.

The phase noise seen by a DDH tool due to a 1% process variation of a long edge feature (again an edge

longer than the Rayleigh resolution), seen as the difference image between two die, can be estimated as 1% of the line size and height times the Rayleigh resolution divided by the area the diffraction limit spreads the equivalent phase over (just the Rayleigh resolution squared). This assumes that the dimensional change is sub-resolution for the imaging optics. Writing this as an equation, the equivalent phase noise in radians is given by:

$$\delta\phi_p = ((\delta wh) + (w\delta h))/(\delta R\lambda) \quad (11)$$

Where w is the line-width, δw is the change in the line-width due to process variation between the two die, h is the line-height, and δh is the change in the line height due to process variation between the two die. Substituting wavelength divided by numerical aperture for the Rayleigh resolution gives:

$$\delta\phi_p = ((\delta wh) + (w\delta h))NA/(\lambda^2) \quad (12)$$

As an example, assume a 1% process variation, a 130 nm line-width, a 500 nm line-height, a 0.5NA imaging optic, and the previously assumed 266 nm wavelength illumination. Then the calculated phase noise is 0.53 degrees (0.0092 radians). Using wavelength to convert this phase to an equivalent height, the equivalent one-sigma defect height would be 0.39 nm. Clearly, a 1% process variation would not be a large source of noise in this case. Even a 10% process variation taken at the three-sigma level would be equivalent to a ~12 nm defect, still not significant. Process variation is nominally not expected to be a significant noise source for small feature sizes. Taken over larger feature sizes, a 10% neighboring-die process variation could start to be a problem. For instance a just-resolved 300 nm line with a 10% variation of a 1-micron line height would look like a defect of 300 nm by 300 nm by 100 nm in phase volume, or a 96 nm cube defect.

Photon Statistical Noise

Phase Noise

The fractional standard deviation of the phase due to photon statistics is given by (see Ref. 7 page 235, and modify for photon holograms rather than electron holograms):

$$\sigma_p = \frac{\sqrt{2}}{\mu ppf \sqrt{N}} \quad (13)$$

Where μ is the actual fringe contrast of the carrier-frequency fringes for the hologram (typically 40% to 50% for the DDH tool), ppf is the pixels per carrier frequency fringe for the camera magnification, and N is the average number of (coherent) photons detected (not incident, but actually detected) per pixel or photoelectrons per pixel. This represents the Poisson statistics (photon statistics) uncertainty in the positional measurement of a single fringe (one wavelength) due to photon statistics. As an example, for 250,000 average photoelectrons (detected photons) per pixel at that particular fringe location, and 2.7 pixels per fringe and a fringe contrast of 0.90 (90%) at the specified location, the uncertainty in the phase is 0.0012 or 0.1% of a wavelength. While these are all high numbers, they are not impossibly high numbers, so that reaching a sensitivity of ~1/1000'th of a wavelength is a possible goal. Note that the phase noise will have a positional dependence in the hologram if the coherent photons detected and/or the fringe contrast varies.

Amplitude Noise

The photon statistics uncertainty in the amplitude (electric field measurement) is given by the similar expression for the amplitude, see Ref. 7. Amplitude uncertainties may be dominated by the ability to normalize out DC amplitude fluctuations, rather than photon statistics.

SIGNAL TO NOISE RATIO AND SENSITIVITY

Given the phase noise as a fraction of the wavelength, it is possible to estimate the minimum expected phase signal for a particular specified defect and thereby estimate the expected signal to noise ratio. The expected signal can be estimated using either the diffraction-corrected phase estimate and assuming like material on like material (no optical properties difference between the defect and the background materials) or given the optical properties of all materials involved then the TL equations can be used along with simple diffraction theory to estimate the signal, and then the signal to noise ratio (SNR) for a particular NA imaging system at illumination wavelength λ . The ratio of the signal to the noise

standard deviation required to keep false counts down to an acceptable level can also be estimated if the spatial frequency of the noise is known or estimated and a Gaussian (normal) noise distribution is assumed

TABLE 1. Noise and Sensitivity, Defect Material Identical to Background Material, 266 nm illumination.

Objective	Sensitivity— Noise=1.4%, SNR=4	Sensitivity— Noise=0.84% SNR=4	Sensitivity— Noise=0.45% SNR=4.0
0.5 NA	55 nm	41 nm	31 nm
0.2 NA	136 nm	102 nm	76 nm
0.1 NA	270 nm	165 nm	152 nm

Table 1 shows the expected defect sensitivity of the phase measurement for various objectives and assuming various noise levels, for an illumination wavelength of 266 nm. This particular table assumes defect material same as background material—for background materials with a different index of refraction from the defect the sensitivity can be greatly increased. The first column assumes a phase noise of 1.4% of a wavelength, a signal to noise ratio of four, and a defect that has dimension x by $1.5x$ by 500 nm height, for instance a scallop in a line or trench (remembering that the phase measurement really measures a defect volume). The second column is similar with an assumed noise of 1% of a wavelength, and the third column assumes that the noise is 0.45% of a wavelength, just slightly larger than the expected photon statistics noise.

It should be emphasized again that Table 1 is for the defect material being identical to the background material. **For small defects with different optical properties than the background material, the sensitivity is usually greatly increased.**

EXAMPLES—HARI AND PHASE OBJECTS

Some examples of defects seen with the DDH Fathom tool are shown below.

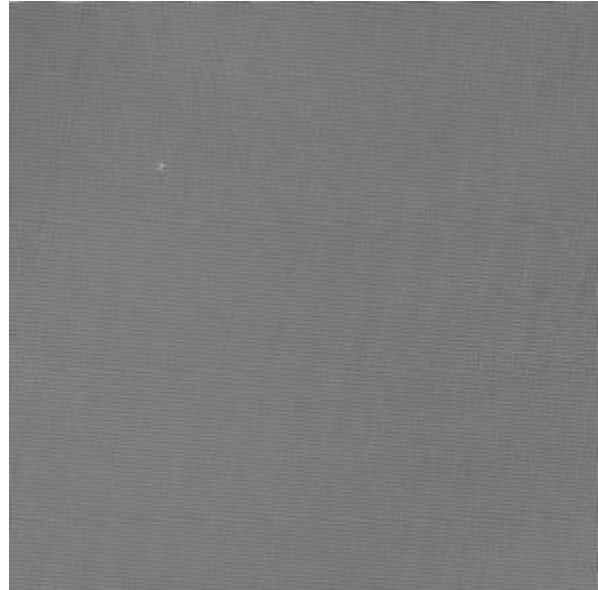


FIGURE 13. Phase image from a 266 nm DDH tool showing a single bad contact in a field of more than 10,000 good contacts. Wafer provided by International SEMATECH.

Figure 13 shows the phase image from a hologram of an array of contacts. A single bad contact is clearly visible in the array of good contacts. The contacts in the array are ~220 nm diameter on a 540 nm pitch. The contacts are all approximately 1500 nm deep. The good contacts all penetrate down to Si, and the bad contact has a layer of approximately 50 nm of SiO₂ at the bottom over the Si. Signal from the bad contact relative to the good contacts is greatly enhanced due to the difference in optical properties between Si and SiO₂.

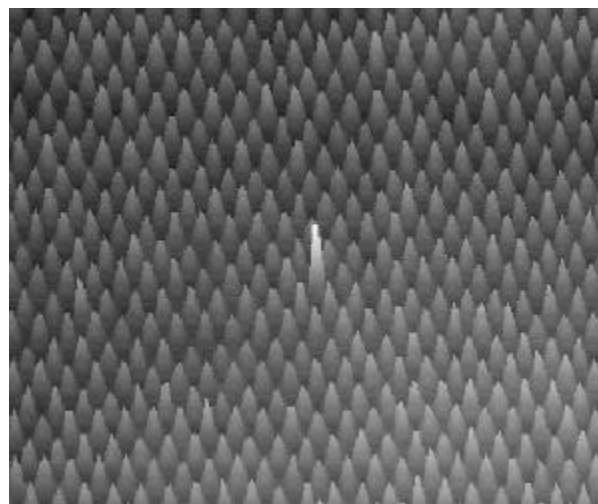


FIGURE 14. This is a 3D phase image showing a single bad contact in a wafer contact layer.

Figure 14 is a different example of a single bad contact in an array of contacts. In this case the phase image is plotted as a true 3D plot of the relative phase signal from the contacts. The contacts were approximately 200 nm in diameter at the top.

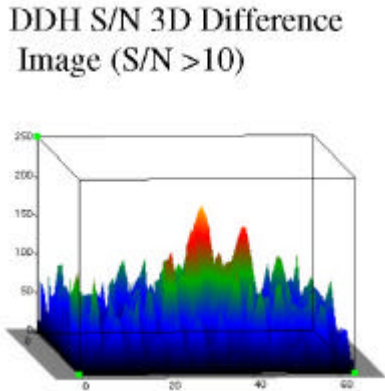


FIGURE 15. Difference image produced when a single bad contact signal with 60 nm defect at the bottom was subtracted from the holographic signal of a good contact.

Figure 15 shows the difference image produced by the DDH tool when the complex image of an array with a bad contact having a ~60 nm defect at the bottom was subtracted from the complex image of an array of good contacts.

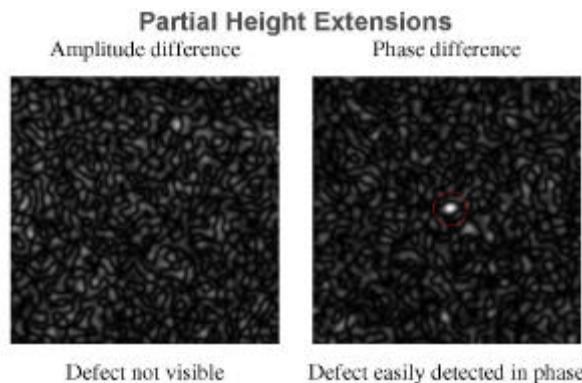


FIGURE 16. Partial height extension is invisible in amplitude but easily detected in phase.

The phase sensitivity of the DDH technology is one of its major advantages. Figure 16 shows another example of this sensitivity. Partial height defects of the same or similar material as the background material (*e.g.*, oxide defect on oxide background) are difficult to detect on conventional brightfield tools because they are primarily found by edge effects. Figure 16 displays the difference image where a field with a partial height defect was subtracted from the similar good field. The defect shows up strongly in

the phase difference, but is invisible in the amplitude difference.

CONCLUSION

In summary, the DDH technology shows tremendous potential as a tool for semiconductor process diagnostics and for general metrology and comparison of wavelength and sub-wavelength features.

ACKNOWLEDGMENTS

The research leading to this paper was initially funded by the United States Department of Energy at Oak Ridge National Laboratory. The assistance of the National Institute of Standards and Technology's Advanced Technology Program to nLine Corporation and its Joint Venture Partners has been and continues to be a crucial part of the development of the DUV Alpha Tools, and for exploring wafer materials and interactions with DUV lasers and optics. The assistance of International SEMATECH in providing wafers, consultation, and other valuable assistance is gratefully acknowledged. The continued support of nLine Corporation's investors is even more gratefully acknowledged.

REFERENCES

1. Gabor, D., *Proc. Roy. Soc. London Ser. A* **A197**, p. 459 (1949).
2. Leith, E., and Upatnieks, J., *J. Opt. Soc. Am.* **52**, p. 1123 (1962).
3. Leith, E., and Upatnieks, J., *J. Opt. Soc. Am.* **53**, p. 1377 (1963).
4. Heflinger, L. O., Wuerker, R. F., and Brooks, R. E., *J. App. Phys.*, **37**, p. 643 (1966).
5. Thomas, C. E., et. al., "Direct to Digital Holography and Holovision", U.S. Patent 6,078,392, June 20, 2000. Other patents applied for.
6. Thomas, C. E., and Hanson, G. R., "Acquisition and Replay Systems for Direct-to-Digital Holography and Holovision", U.S. Patent 6,525,821, Feb. 25, 2003. Other patents applied for.

7. Voelkl, E., Allard, L.F., and Joy, D. C., *Introduction to Electron Holography*, New York: Kluwer Academic/Plenum Publishers, 1999, Chapter 6, and other.
8. Ramo, S., Whinnery, J. R., and Van Duzer, T., *Fields and Waves in Communication Electronics, Second Edition*, New York: John Wiley & Sons, 1984, Chapter 5.
9. Church, E. L., and Lange, S. R., *Structure effects in optical surface metrology*, SPIE Vol. 680, Surface Characterization and Testing (1986).
10. Born, M., and Wolf, E., *Principles of Optics, Seventh (expanded) Edition*, Cambridge: Cambridge University Press, 1999, p. 737 and following, note: caution! k in the present work is identified as κ in Born and Wolf.
11. Yariv, A., *Optical Electronics, 3rd Edition*, New York: Holt, Rinehart and Winston, 1985, Chapter 13, pp 449-453.
12. Gamelin, J., Guerrieri, R., Tadros, K., Wong, A., Pistor, T., Doi, T., Hall, E. *Tempest User's Guide, version 5.1*, Berkeley: University of California Berkeley, 1998, see http://cuervo.eecs.berkeley.edu/Volcano/www/sim_manual.html
13. Pistor, T. V., *Electromagnetic Simulation and Modeling With Applications In Lithography*, Ph.D. Thesis, Memorandum No. UCB/ERL M01/19, May 1, 2001.
14. <http://www.panoramictech.com>.
15. Wurtz, G. A., Dimitrijevic, N. M., Wiederrecht, G. P., *Jpn. J. Appl. Phys*, **41**, pp L351-L354 (2002), see Fig. 3 and Fig. 4.
16. Stover, J. C., *Optical Scattering: Measurement and Analysis, second edition*, Bellingham: SPIE OPTICAL ENGINEERING PRESS, 1995, Chapter 1.
17. Phillips Imaging, *Product Information, FTF2020-M, Full-Frame CCD Image Sensor*, Eindhoven, Netherlands, 1998.
18. CLAS 2D Shack-Hartmann Wavefront Sensor, Wavefront Sciences Incorporated, 14810 Central Avenue SE, Albuquerque, NM 87123-3932 Tel: (505)275-4747